CHAPTER 3

SINGLE EVACUATED TUBE THERMOSYPHON MODEL

This chapter will present the experiment of the evacuated tube solar water heater using thermosyphon which filled with refrigerant R141b as working fluid compared with industrial thermosyphon. Both thermosyphons are tested under the same tilt angle, water flow rate, and identical weather condition. In order to design mathematical models, solar intensity and ambient air temperature of the experiment are applied to the model. Furthermore, the thermal resistance method and Finite Difference Method (FDM) are brought to predict the temperature, heat rate of water of storage tank, and thermal efficiency. The results of both mathematical models are validated with the experimental results.

3.1 Experimental setup

In this study, the single evacuated tube solar water heater using industry thermosyphon and refrigerant thermosyphon is investigated. It consists of evacuated tube, two-phase thermosyphon, and water storage tank. The structure of evacuated tube is 58 mm of outer tube diameter, 47 mm of inner tube diameter, and 1800 mm of total length and other specifications of evacuated tube as shown in Table A-1.

Two-phase thermosyphons are made of copper tube. Since the outside diameter of evaporator section and condenser section are 8 mm and 14 mm, their length are 1700 mm and 80 mm, respectively. The refrigerant thermosyphon is filled R141b as the filling ratio about 70% of evaporator volume. For the working fluid of industrial thermosyphon is filled by the water and copper powder. The thermosyphon and collector fin are inserted into the evacuated tube between the inner wall tubes. The amount of water storage within the tank is about 50 liters while the water flow rate is circulated to a manifold by pump about 0.03 kg/s (Nada et al., 2004). Therefore, the evacuated tube collectors are set on the stand, tilted 18^{o} from horizontal and facing to south as shown in Figure 3.1.

Figure 3.1 The experimental setup of the evacuated tube collector with industrial thermosyphon and R141b thermosyphon

Figure 3.2 Thermocouple chromel-alumel (K-Type)

Figure 3.3 Brainchild data logger model VR18

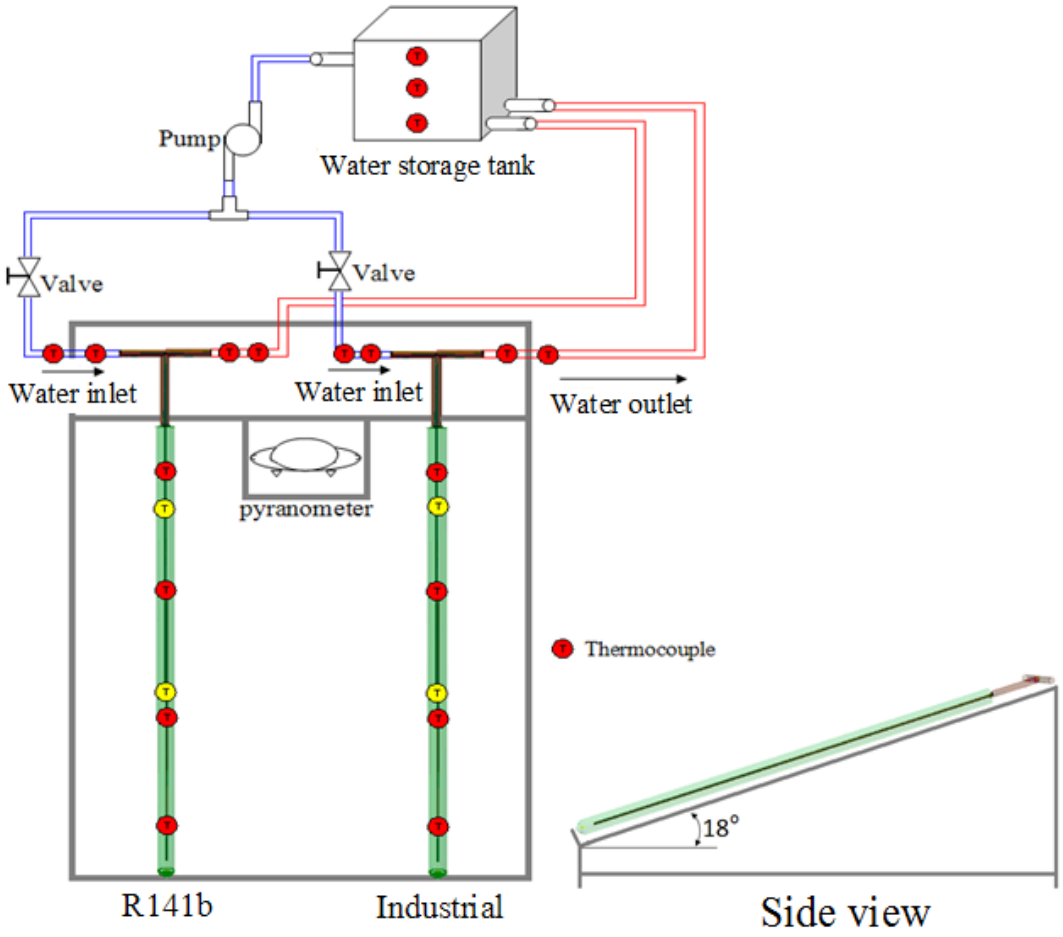

Figure 3.4 Schematic of the system and mounted measurement of single evacuated tube solar water heater

For the experiments, temperatures are measured in K-type thermocouples. In Figure 3.2, thermocouples operating temperature range of -270^{o}C to 1260^{o}C and accuracy of ± 1.1^{o}C are connected to Brainchild model VR18 data logger for temperature recording as shown in Figure 3.3. Moreover, Kipp & Zonen pyranometer model CMP3 is based on solar intensity measurement which its sensitivity is 19.11 x 10^{-6} V/Wm^{-2} and error is ±1%. Pyranometer is set on the surface that parallel with the tilt angle of the solar collector without casting shadow. The schematic diagram of the single evacuated tube solar water heater and setting measurement are illustrated in Figure 3.4.

The radiation shield covering the single solar collector is removed at 09:00 a.m. and the experiment is carried out from 9:00 a.m. to 4:00 p.m. Each day, hot water stored in tank is drained in the morning and filled with cold water in temperature about 27^{o}C. The experiments are tested under the climatic conditions of Chiang Mai, Thailand.

The radiation shield covering the single solar collector is removed at 09:00 a.m. and the experiment is carried out from 9:00 a.m. to 4:00 p.m. Each day, hot water stored in tank is drained in the morning and filled with cold water in temperature about 27^{o}C. The experiments are tested under the climatic conditions of Chiang Mai, Thailand.

3.2 Mathematical model

Mathematical models are presented and divided into two parts: the first one is the mathematical model using a principle of thermal resistance while the second one is the mathematical model using Finite Difference Method (FDM). MATLAB program is employed for the modeling of both mathematical models in order to predict temperature, heat rate of water, and thermal efficiency of single tube solar water heater. Then, the mathematical models are used for investigating the accuracy by using the experimental results of the single evacuated tube solar water heater.

3.2.1 Mathematical model assumptions

In order to predict the evacuated tube solar water heater system, assumptions, control parameters, and boundary conditions are defined as followings.

3.2.1.1 Assumptions of the single evacuated tube solar water heater:

1) Solar radiation incident on the surface of evacuated tube collector in all directions.
2) Heat loss of the thermosyphon at adiabatic section is negligible.
3) Z_4, Z_5 and Z_6 of thermosyphon are usually neglected due to their relatively small in magnitude.
4) Solar radiation and ambient temperature are based on Chiang Mai, Thailand.

3.2.1.2 Controlled parameters of the single evacuated tube solar water heater:

1) The evacuated tube data as show in Table A-1.
2) Thermosyphon is made of copper tube and R141b is filled about thermosyphon in 70% of evaporator volume.
3) Length of evaporator, adiabatic, and condenser are 1700 mm, 50 mm, and 80mm, respectively.
4) Diameter of evaporator and adiabatic are 8 mm.
5) Diameter of condenser is 14 mm.
6) Volume water storage tank is 50 liters.
7) Water flow rate is 0.03 kg/s (Nada et al., 2004).

3.2.1.3 Boundary conditions of the single evacuated tube solar water heater:

1) The outer collector fin temperature (T_{o_fin}) is equal to the inner evacuated tube temperature (T_{i_g}) as shown in Figure 3.5.
2) The outer evaporator section temperature (T_{evap}) is equal to the inner collector fin temperature (T_{i_fin}) as shown in Figure 3.5.
3) Water outlet temperature of manifold (T_{wo_m}) is equal to water inlet temperature of water storage tank (T_{wi_tank}).
4) Water inlet temperature of the manifold (T_{wi_m}) is equal to water outlet temperature of water storage tank (T_{wo_tank}).

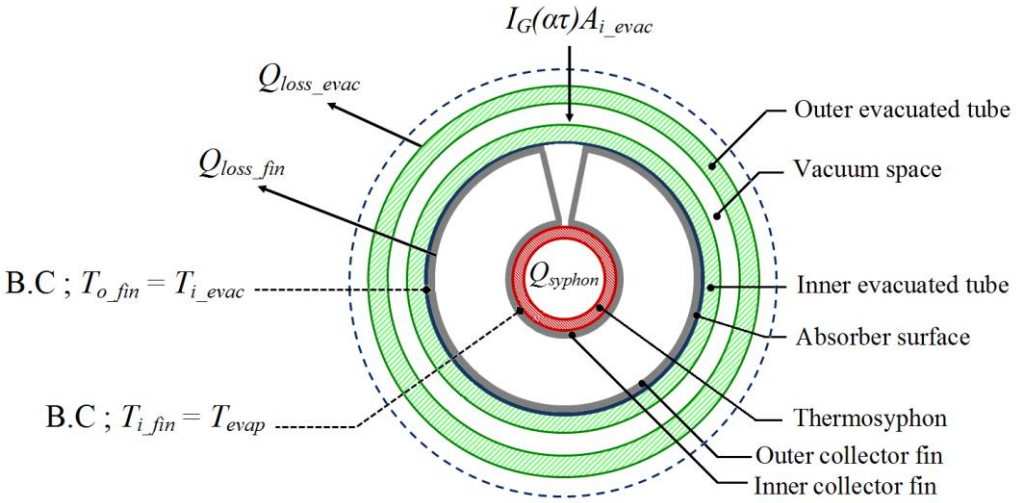

Figure 3.5 Boundary conditions of temperatures

3.2.2 Thermal resistance method

Thermal resistance method for single evacuated tube with thermosyphon can be exhibited in electric resistance form as shown in Figure 3.6

3.2.2.1 Evacuated tube

The solar radiation incident on the surface of evacuated tube collector, so it is transmitted through the outer evacuated tube wall thereafter it is absorbed by the absorber surface which coated inside of inner evacuated tube. Applying the energy balance on the evacuated tube is illustrated as in Equation 3.1.

$$\dot{Q}_{ST\_evac} = I_G(\tau\alpha)A_{o\_evac} - \dot{Q}_{loss\_evac} \tag{3.1}$$

Where I_G is solar radiation as the heat per area (W/m^2), τ is transmittance of glass tube, α is absorptance of absorber surface, A_{o_evac} is glass tube area (m^2), $\dot{Q}_{loss\_evac}$ is heat loss of evacuated tubes to surrounding due to temperature difference of outer evacuated tube temperature ($T^n_{o\_evac}$) with ambient temperature (T^n_{am}). It can be calculated by

$$\dot{Q}_{loss\_evac} = h_{air}A_{o\_evac}(T^n_{o\_evac} - T^n_{am}) \tag{3.2}$$

Where A_{o_evac} is outer surface area of an evacuated tube (m^2), h_{air} is the convection heat transfer coefficient (W/m^2-K).

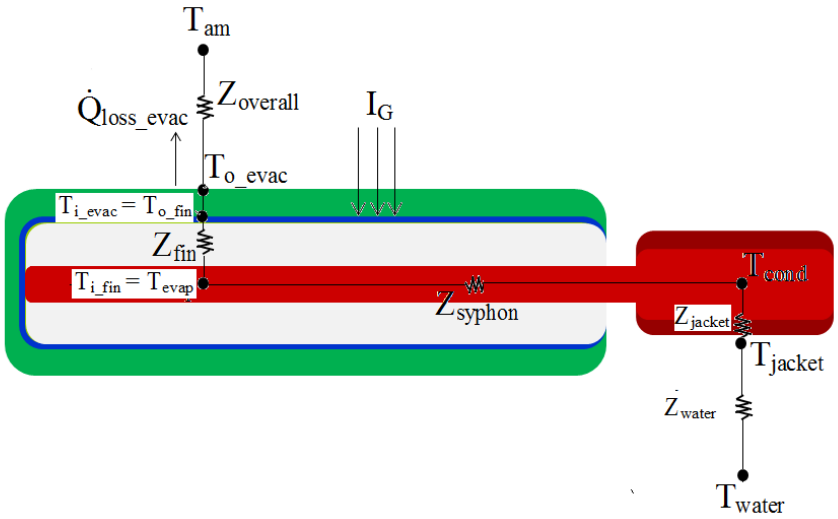

Figure 3.6 Thermal resistance of the evacuated tube with thermosyphon

Wind velocity is used for calculating heat transfer coefficient (h_{air}) from Reynolds number (Re) and Nusselt number (Nu) by Churchill and Bernstein (Cengel, 2004) as follows:

$$Nu_d = \frac{h_{air} D_{o\_evac}}{k_{o\_evac}} = 0.3 + \frac{0.62\, Re_d^{1/2}\, Pr_{air}^{1/3}}{\left[1+\left(\frac{0.4}{Pr_{air}}\right)^{2/3}\right]^{1/4}} \left[1+\left(\frac{Re_d}{282{,}000}\right)^{5/8}\right]^{4/5} \tag{3.3}$$

The Reynolds number (Re_d) is expressed as follow:

$$Re_d = \frac{\rho_{air} V_{wind} D_{o\_evac}}{\mu_{air}} \tag{3.4}$$

Inner evacuated tube temperature at the present time ($T_{i\_evac}^{n}$) can be solved by converting radiation heat transfer in two-surface enclosures as follow:

$$T_{i\_evac}^{n} = \sqrt[4]{\frac{\left(\dot{Q}_{ST\_evac}\right)\left(\frac{1}{\varepsilon_{i\_evac}} + \frac{r_{i\_evac}}{r_{o\_evac}}\left(\frac{1-\varepsilon_{o\_evac}}{\varepsilon_{o\_evac}}\right)\right)}{\sigma A_{i\_evac}} + \left(T_{o\_evac}^{n}\right)^4} \tag{3.5}$$

σ is the Stefan–Boltzmann constant (W/m^2-K^4), ε is the emissivity of outer and inner surface of evacuated tube.

Cumulative thermal energy at absorber surface ($\dot{Q}_{ST\_evac}$), temperature condition of the inner evacuated tube ($T^n_{i\_evac}$) is equal to the outer collector fin ($T^n_{o\_fin}$) in the previous boundary condition are applied in order to calculate the collector fin temperature.

3.2.2.2 Collector fin

For consider the collector fin in this study, from Figure 3.6, it can see that the shape of collector fin similar the cylindrical ring. Thus, in this study, the calculation of the collector fin is assumed to the cylindrical ring. From the previous boundary conditions, outer collector fin temperature ($T^n_{o\_fin}$) is brought to calculate with inner collector fin temperature ($T^n_{i\_fin}$) by thermal resistance as follow:

$$T^n_{i\_fin} = T^n_{o\_fin} - (\dot{Q}_{ST\_evac})(Z_{fin}) \tag{3.6}$$

Z_{fin} is thermal resistance between outer and inner collector fin (K/W) calculated by

$$Z_{fin} = \frac{ln(D_{o\_fin} / D_{i\_fin})}{2\pi L_{fin} k_{fin}} \tag{3.7}$$

D_{o_fin} and D_{i_fin} are outer and inner diameter collector fin (m), L_{fin} is collector fin length, and k_{fin} is thermal conductivity of collector fin (W/m-K). Substitution of Equation (3.7) by Equation (3.6), is obtain inner collector fin temperature ($T^n_{i\_fin}$). After that the inner collector fin temperature is assumed equal to the temperature of themsyphon at evaporator section (T^n_{evap}).

3.2.2.3 Thermosyphon

The heat transfer of thermosyphon can be calculated by thermal resistances as shown in Figure 2.8. It includes evaporator and condenser wall resistance (Z_2, Z_8), working fluid resistance (Z_3, Z_7), and thermal resistance along axial length of the thermosyphon wall (Z_{10}). Thus, total thermal resistance of thermosyphon consists of Z_2, Z_3, Z_7, Z_8, and Z_{10} which it can be calculated from Equation (2.2) to Equation (2.14).

The overall thermal resistance (Z_{tot}) can be calculated from Equation (2.16) or Equation (2.17). Then, the condenser temperature (T_{cond}^{n}) can be obtained as follows.

$$T_{cond}^{n} = T_{evap}^{n} - (\dot{Q}_{syphon})(Z_{tot}) \tag{3.8}$$

Where T_{evap}^{n} is evaporator temperature (K) and Z_{tot} is overall thermal resistance (K/W).

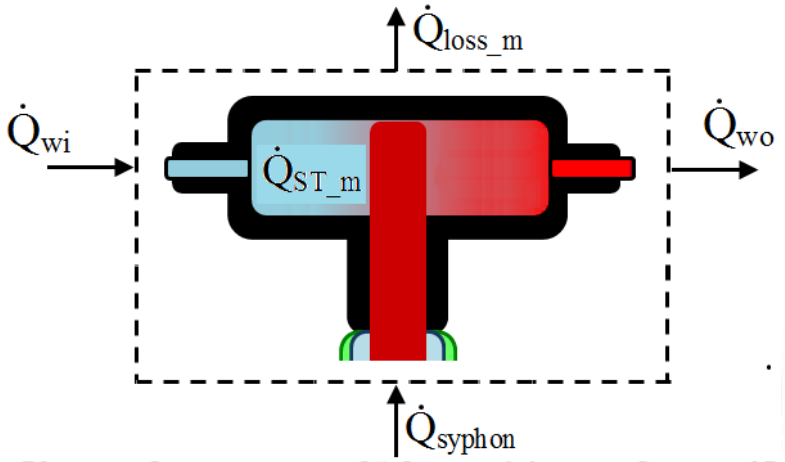

Figure 3.7 Control volume of the manifold

3.2.2.4 Manifold

Considering the heat transfer rate of water at the manifold is applied for the solar water heater, the conservation of energy at the manifold as shown in Equation (3.9) and the control volume of the manifold as shown in Figure 3.7. Heat of thermosyphon ($\dot{Q}_{syphon}$) is divided into two parts i.e. transferred to manifold which water flows around condenser section of thermosyphon and heat loss to surrounding by convection heat transfer. Then, the heat is removed to water by convection. Energy balance of the manifold is

$$\dot{Q}_{ST\_m} = \dot{Q}_{syphon} + \dot{Q}_{wi} - \dot{Q}_{wo} - \dot{Q}_{loss\_m} \tag{3.9}$$

Heat transfer rate of water ($\dot{Q}_{ST\_m}$) at the manifold can be calculated from

$$\dot{Q}_{ST\_m} = \frac{M_{w\_m} c_p (T^n_{w\_m} - T^{n-1}_{w\_m})}{\Delta t} \tag{3.10}$$

Substitution of Equation (3.10) by Equation (3.9) and calculating water temperature within the manifold at the present time ($T^n_{w\_m}$) from

$$T^n_{w\_m} = \frac{(\dot{Q}_{syphon} + \dot{Q}_{wi} - \dot{Q}_{wo} - \dot{Q}_{loss\_m})\Delta t}{M_{w\_m} c_p} + T^{n-1}_{w\_m} \tag{3.11}$$

Where M_{w_m} is water mass within the manifold (kg), c_p is specific heat of water at constant pressure (J/kg-K), $T^{n-1}_{w\_m}$ is water temperature within the manifold at the previous time (^{o}C), Δt is the interval storage time (s), $\dot{Q}_{wi}$ and $\dot{Q}_{wo}$ are the heat rate of water inlet and outlet the manifold which is referred to the net heat rate of manifold ($\dot{Q}_{io\_m}$). The net heat rate of water at the manifold can be calculated by temperature difference of water inlet and outlet at the manifold multiplied by the water flow rate and by the specific heat of water, it follows that

$$\dot{Q}_{io\_m} = \dot{m}_w c_p (T^n_{wo\_m} - T^n_{wi\_m}) \tag{3.12}$$

Where $\dot{m}_w$ is water flow rate (kg/s), $T^n_{wi\_m}$ is inlet temperature of water at manifold and $T^n_{wo\_m}$ is outlet temperature of water at manifold which assumed that it is equal to temperature of water within the manifold ($T^n_{w\_m}$) at the same time.

From Equation (3.9), heat loss of water within the manifold ($\dot{Q}_{loss\_m}$) to surrounding is calculated by natural convection heat transfer at the outer surface of manifold as follow:

$$\dot{Q}_{loss\_m} = h_{air} A_m (T^n_{s\_m} - T^n_{am}) \tag{3.13}$$

A_m is outer surface area of manifold (m^2), h_{air} is natural convection heat transfer coefficient (W/m^2-K), and $T^n_{s\_m}$ is the average surface temperature of manifold which can be determined by ($T^n_{w\_m} + T^n_{am}$) / 2.

3.2.2.5 Water storage tank

For water storage tank, the heat is accumulated within water at the manifold and then flows to the water storage tank. Applying energy balance on controlled volume as shown in Figure 3.8:

$$\dot{Q}_{ST\_tank} = \dot{Q}_{wi\_tank} - \dot{Q}_{wo\_tank} - \dot{Q}_{loss\_tank} \tag{3.14}$$

The accumulated heat rate of water at storage tank ($\dot{Q}_{ST\_tank}$) can be calculated as follow

$$\dot{Q}_{ST\_tank} = \frac{M_{w\_tank} c_p (T^{n}_{w\_tank} - T^{n-1}_{w\_tank})}{\Delta t} \tag{3.15}$$

M_{w_tank} is water mass within the storage tank (kg), $T^{n}_{w\_tank}$ is temperature of water in the storage tank at the present time (^{o}C), $T^{n-1}_{w\_tank}$ is temperature of water in the storage tank at the previous time (^{o}C), and Δt is the interval time (s)

Heat loss of water storage tank to surrounding ($\dot{Q}_{loss\_tank}$) occurred from the temperature difference of water temperature in storage tank and ambient air temperature can be calculated by

$$\dot{Q}_{loss\_tank} = \frac{T^{n}_{w\_tank} - T^{n}_{am}}{Z_{tank}} \tag{3.16}$$

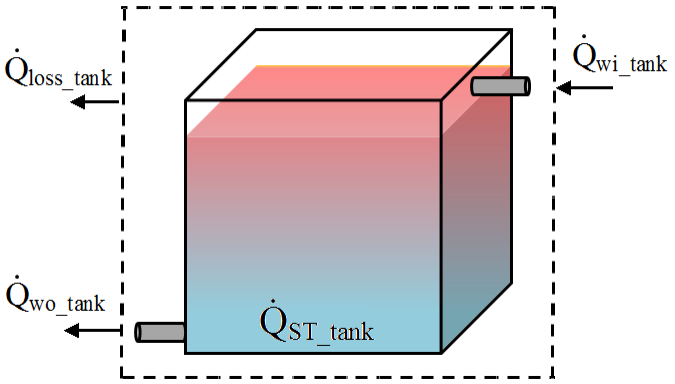

Figure 3.8 Controlled volume of the storage tank

$$Z_{tank} = \left(\frac{t_{tank}}{A_{tank}k_{tank}}\right) + \left(\frac{t_{ins}}{A_{ins}k_{ins}}\right) + \left(\frac{1}{h_{air}A_{ins}}\right) \tag{3.17}$$

Where t_{tank} is wall thickness of storage tank (m), t_{ins} is insulator thickness (m), A_{tank} and A_{ins}, is area of the water storage tank or area of the insulated (m^2), k_{tank} and k_{ins} is the thermal conductivity of storage tank and insulated (W/m-K), respectively.

The heat rate of water inlet ($\dot{Q}_{wi\_tank}$) and water outlet ($\dot{Q}_{wo\_tank}$) the storage tank which is referred to the net heat rate of storage tank ($\dot{Q}_{io\_tank}$). The net heat rate of water at the storage tank can be calculated by:

$$\dot{Q}_{io\_tank} = \dot{m}_w c_p (T^n_{wi\_tank} - T^n_{wo\_tank}) \tag{3.18}$$

$T^n_{wi\_tank}$ is inlet temperature of water at the storage tank and $T^n_{wo\_tank}$ is outlet temperature of water at the storage tank which assumed that it is equal to the temperature of water within the water storage tank ($T^n_{w\_tank}$) at the same interval time.

Thermal efficiency of solar water heater system is described as following formula

$$\eta_{system} = \frac{\dot{Q}_{ST\_tank}}{I_G(\tau\alpha)A_{o\_evac}} \tag{3.19}$$

The flow chart of thermal resistance modeling of the single evacuated tube solar water heating with thermosyphon is described in Figure 3.9

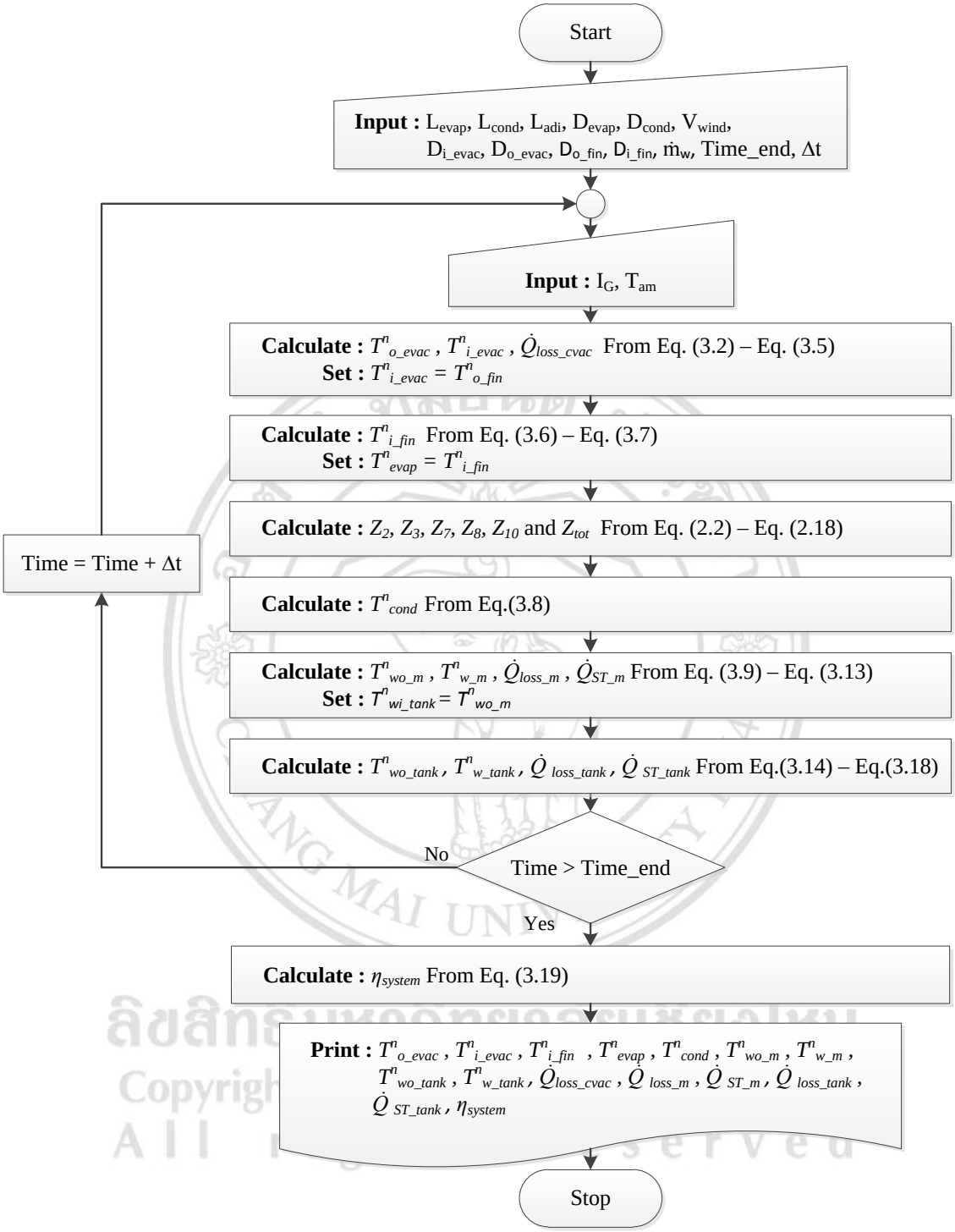

Figure 3.9 Computational step of thermal resistance method

3.2.3 Explicit Finite Difference Method

The Explicit Finite Difference Method (EFDM) approach is employed to predict temperatures, heat transfer rate, and thermal efficiency of the single evacuated

tube solar water heater system. The conservation of energy is applied to the domains and considered in r-θ-z direction, as following formula:

$$\frac{1}{\alpha}\frac{\partial T}{\partial t} = \nabla^2 T + \frac{\dot{q}}{k} = \frac{\partial^2 T}{\partial r^2} + \frac{1}{r}\frac{\partial T}{\partial r} + \frac{1}{r^2}\frac{\partial^2 T}{\partial \theta^2} + \frac{\partial^2 T}{z^2} + \frac{\dot{q}}{k} \tag{3.20}$$

From Equation (3.20) can be applied in Finite Difference Equation for all domains surface as follows

$$\begin{aligned}\frac{T^{n}_{(r,\theta,z)} - T^{n-1}_{(r,\theta,z)}}{\alpha \Delta t} = {} & \frac{T^{n-1}_{(r+1,\theta,z)} - 2T^{n-1}_{(r,\theta,z)} + T^{n-1}_{(r-1,\theta,z)}}{\Delta r^2} + \frac{1}{\Delta r}\frac{T^{n-1}_{(r+1,\theta,z)} - T^{n-1}_{(r-1,\theta,z)}}{2\Delta r} \\ & + \frac{1}{(\Delta r)^2}\frac{T^{n-1}_{(r,\theta+1,z)} - 2T^{n-1}_{(r,\theta,z)} + T^{n-1}_{(r,\theta-1,z)}}{\Delta \theta^2} \\ & + \frac{T^{n-1}_{(r,\theta,z+1)} - 2T^{n-1}_{(r,\theta,z)} + T^{n-1}_{(r,\theta,z-1)}}{\Delta z^2} - \frac{\dot{q}}{k}\end{aligned} \tag{3.21}$$

Explicit Finite Difference Equation in the Equation (3.21) is modified to each the components of the mathematical model of evacuated tube collector with thermosyphon which is divided into three domains: the evacuated tube, collector fin and thermosyphon. For the each of the component is divided into the annual rings, which consist of outside annual ring (*oar*), inside annual ring (*iar*), and another annual ring (*r*). The sample of the annual ring is shown in Figure 3.10.

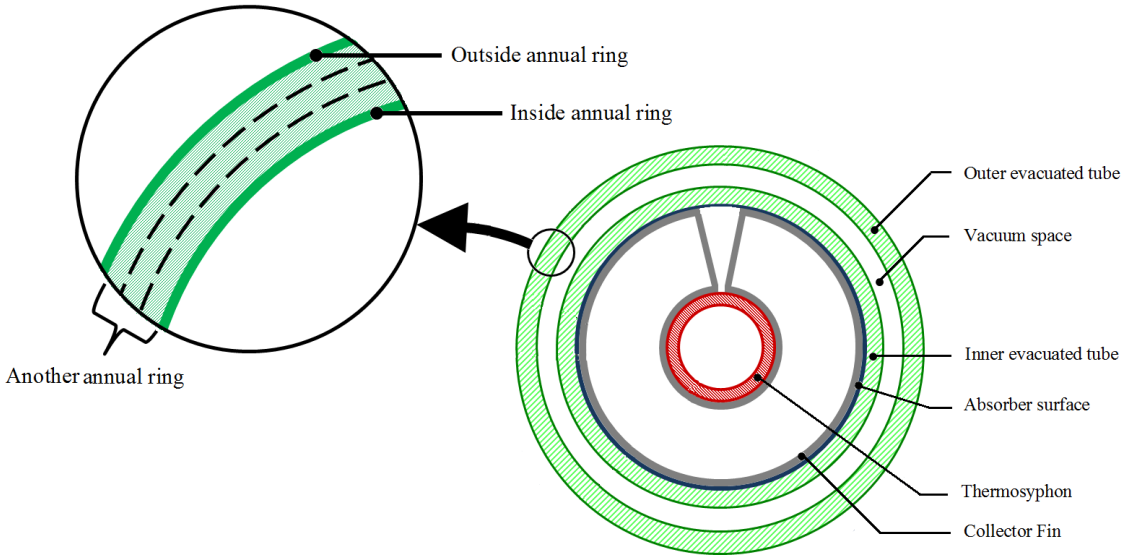

Figure 3.10 The sample of the annual rings

3.2.3.1 Evacuated tube domain

The solar radiation incident on the surface of evacuated tube collector. The solar radiation is transmitted through the outer evacuated tube wall and absorbed by the absorber surface of its inner evacuated tube wall, which is coated with a special selective coating. Applying a conservation of energy on a controlled surface of the evacuated tube as shown in Figure 3.11, it follows that

$$\dot{Q}_{ST\_evac} = I_G(\tau\alpha)A_{i\_evac} - \dot{Q}_{loss\_evac} \tag{3.22}$$

Where I_G is the solar intensity incident on the surface of evacuated tubes (W/m^2), τ is the transmittance of an evacuated tube, α is an absorptivity of absorber surface, A_{i_evac} is an inner surface area of an evacuated tube (m^2). $\dot{Q}_{ST\_evac}$ is the remainder of thermal energy stored in absorber surface (W). $\dot{Q}_{loss\_evac}$ is the heat loss of evacuated tubes to surrounding (W), it is calculated from temperature difference of outer evacuated tube temperature and ambient temperature as follow:

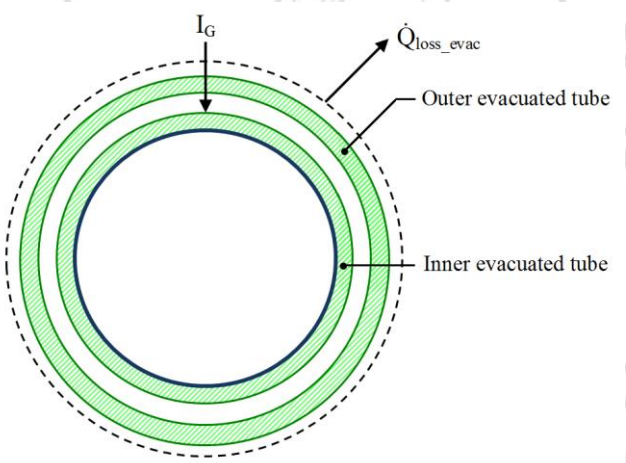

Figure 3.11 Controlled volume of cross-section in the single evacuated tube

$$\dot{Q}_{loss\_evac} = h_{air}A_{o\_evac}(T^n_{o\_evac(oar,\theta,z)} - T^n_{am}) \tag{3.23}$$

Where h_{air} is the convection heat transfer coefficient (W/m^2-K) that is calculated from Equation (3.3).

For outer and inner of the evacuated tube are divided into four annual rings and annual ring thickness which is 0.4 mm of radial step (Δr). Also, EFDM is applied to calculate the outer evacuated tube temperature as follows:

Considering at outside annual ring:

$$\begin{aligned}\frac{T^{n}_{o\_evac(oar,\theta,z)}-T^{n-1}_{o\_evac(oar,\theta,z)}}{\alpha\Delta t} &= \frac{T^{n-1}_{o\_evac(oar+1,\theta,z)}-2T^{n-1}_{o\_evac(oar,\theta,z)}+T^{n-1}_{o\_evac(oar-1,\theta,z)}}{\Delta r^{2}}+\ldots \\ &\frac{1}{\Delta r}\frac{T^{n-1}_{o\_evac(oar+1,\theta,z)}-T^{n-1}_{o\_evac(oar-1,\theta,z)}}{2\Delta r}+\ldots \\ &\frac{1}{(\Delta r)^{2}}\frac{T^{n-1}_{o\_evac(oar,\theta+1,z)}-2T^{n-1}_{o\_evac(oar,\theta,z)}+T^{n-1}_{o\_evac(oar,\theta-1,z)}}{\Delta\theta^{2}}+\ldots \\ &\frac{T^{n-1}_{o\_evac(oar,\theta,z+1)}-2T^{n-1}_{o\_evac(oar,\theta,z)}+T^{n-1}_{o\_evac(oar,\theta,z-1)}}{\Delta z^{2}}+\ldots. \\ &\frac{I_{G}(\tau\alpha)}{k_{evac}\Delta r}-\frac{h_{air}(T^{n}_{o\_evac(oar,\theta,z)}-T^{n}_{am})}{k_{air}\Delta r}\end{aligned} \tag{3.24}$$

Considering at another annual ring:

$$\begin{aligned}\frac{T^{n}_{o\_evac\,(r,\theta,z)}-T^{n-1}_{o\_evac\,(r,\theta,z)}}{\alpha\Delta t} &= \frac{T^{n-1}_{o\_evac\,(r+1,\theta,z)}-2T^{n-1}_{o\_evac\,(r,\theta,z)}+T^{n-1}_{o\_evac\,(r-1,\theta,z)}}{\Delta r^{2}}+\ldots \\ &\frac{1}{\Delta r}\frac{T^{n-1}_{o\_evac\,(r+1,\theta,z)}-T^{n-1}_{o\_evac\,(r-1,\theta,z)}}{2\Delta r}+\ldots \\ &\frac{1}{(\Delta r)^{2}}\frac{T^{n-1}_{o\_evac\,(r,\theta+1,z)}-2T^{n-1}_{o\_evac\,(r,\theta,z)}+T^{n-1}_{o\_evac\,(r,\theta-1,z)}}{\Delta\theta^{2}}+\ldots \\ &\frac{T^{n-1}_{o\_evac\,(r,\theta,z+1)}-2T^{n-1}_{o\_evac\,(r,\theta,z)}+T^{n-1}_{o\_evac\,(r,\theta,z-1)}}{\Delta z^{2}}\end{aligned} \tag{3.25}$$

When considering the inner evacuated tube temperature, the thermal energy stored ($\dot{Q}_{ST\_evac}$) in Equation (3.22) is used to calculate the inner evacuated tube at the outside of an annual ring by radiation heat transfer in two-surface enclosures. Thus, the outside temperature of annual ring an inner evacuated tube at the present time ($T^{n}_{i\_evac(oar,\theta,z)}$) can be calculated as follow:

$$T^{n}_{i\_evac(oar,\theta,z)}=\sqrt[4]{\frac{\left(Q_{ST\_evac}\right)\left(\frac{1}{\varepsilon_{i\_evac}}+\frac{r_{i\_evac}}{r_{o\_evac}}\left(\frac{1-\varepsilon_{o\_evac}}{\varepsilon_{o\_evac}}\right)\right)}{\sigma A_{i\_evac}}+\left(T^{n}_{o\_evac(oar,\theta,z)}\right)^{4}} \tag{3.26}$$

Where σ is the Stefan–Boltzmann constant (W/m^2-K^4), ε is the emissivity of the outer and inner surface of evacuated tube.

Another annual ring can be applied Equation (3.22), it follows that:

$$\frac{T^{n}_{i\_evac(r,\theta,z)} - T^{n-1}_{i\_evac(r,\theta,z)}}{\alpha\Delta t} = \frac{T^{n-1}_{i\_evac(r+1,\theta,z)} - 2T^{n-1}_{i\_evac(r,\theta,z)} + T^{n-1}_{i\_evac(r-1,\theta,z)}}{\Delta r^2} + \ldots$$
$$\frac{1}{\Delta r}\frac{T^{n-1}_{i\_evac(r+1,\theta,z)} - T^{n-1}_{i\_evac(r-1,\theta,z)}}{2\Delta r} + \ldots$$
$$\frac{1}{(\Delta r)^2}\frac{T^{n-1}_{i\_evac(r,\theta+1,z)} - 2T^{n-1}_{i\_evac(r,\theta,z)} + T^{n-1}_{i\_evac(r,\theta-1,z)}}{\Delta\theta^2} + \ldots \quad (3.27)$$
$$\frac{T^{n-1}_{i\_evac(r,\theta,z+1)} - 2T^{n-1}_{i\_evac(r,\theta,z)} + T^{n-1}_{i\_evac(r,\theta,z-1)}}{\Delta z^2}$$

From the boundary condition, the inside of annual rings temperature of the inner evacuated tube ($T^{n}_{i\_evac\ (iar,\theta,z)}$) is assumed to be equal to the temperature outside of annual rings at the outer collector fin ($T^{n}_{o\_fin\ (oar,\theta,z)}$).

3.2.3.2 Collector fin domain

The collector fin is inserted into the clearance between the inner evacuated tube wall of double-layer tube and at one end is sealed by a silicone stopper. The heat accumulated at absorber surface is transferred to collector fin. After that, the temperature of collector fin surface is increased. The heat of collector fin is divided into two parts, i.e. accumulated heat at collector fin surface and heat loss to the inside air of evacuated tube by convection heat transfer. The inside air temperature of evacuated tube ($T_{air\_i\_evac}$) increases by increasing the collector fin surface temperature. The temperature of inside air of evacuated tube increasing, the heat accumulated at the silicone stopper and then the silicone stopper converted to the heat loss by convection heat transfer to ambient air. However, heat loss at silicone stopper is less than heat transfer of collector fin. Thus, heat loss at silicone stopper can be negligible.

In this work, the outer and inner of collector fin is divided into three annual rings and the thickness of an annual ring is 0.01 mm of radial step (Δr). At the outside annual ring of the outer collector fin, the boundary condition of temperature of

outer collector fin ($T^{n}_{o\_fin\ (oar,\theta,z)}$) is equal to temperature of the annual rings inside of inner evacuated tube ($T^{n}_{i\_evac\ (iar,\theta,z)}$). From Equation (3.21) and the sample of annual ring in Figure 3.10, another annual ring of outer collector fin has heat conduction and heat loss convection at the inside annual rings of an outer collector fin, it follows that:

Considering at another annual ring:

$$\begin{aligned}\frac{T^{n}_{o\_fin\ (r,\theta,z)} - T^{n-1}_{o\_fin\ (r,\theta,z)}}{\alpha\Delta t} = {} & \frac{T^{n-1}_{o\_fin\ (r+1,\theta,z)} - 2T^{n-1}_{o\_fin\ (r,\theta,z)} + T^{n-1}_{o\_fin\ (r-1,\theta,z)}}{\Delta r^{2}} + \ldots \\ & \frac{1}{\Delta r}\frac{T^{n-1}_{o\_fin\ (r+1,\theta,z)} - T^{n-1}_{o\_fin\ (r-1,\theta,z)}}{2\Delta r} + \ldots \\ & \frac{1}{(\Delta r)^{2}}\frac{T^{n-1}_{o\_fin\ (r,\theta+1,z)} - 2T^{n-1}_{o\_fin\ (r,\theta,z)} + T^{n-1}_{o\_fin\ (r,\theta-1,z)}}{\Delta\theta^{2}} + \ldots \\ & \frac{T^{n-1}_{o\_fin\ (r,\theta,z+1)} - 2T^{n-1}_{o\_fin\ (r,\theta,z)} + T^{n-1}_{o\_fin\ (r,\theta,z-1)}}{\Delta z^{2}}\end{aligned} \tag{3.28}$$

Considering at inside annual ring:

$$\begin{aligned}\frac{T^{n}_{o\_fin\ (iar,\theta,z)} - T^{n-1}_{o\_fin\ (iar,\theta,z)}}{\alpha\Delta t} = {} & \frac{T^{n-1}_{o\_fin\ (iar+1,\theta,z)} - 2T^{n-1}_{o\_fin\ (iar,\theta,z)} + T^{n-1}_{o\_fin\ (iar-1,\theta,z)}}{\Delta r^{2}} + \ldots \\ & \frac{1}{\Delta r}\frac{T^{n-1}_{o\_fin\ (iar+1,\theta,z)} - T^{n-1}_{o\_fin\ (iar-1,\theta,z)}}{2\Delta r} + \ldots \\ & \frac{1}{(\Delta r)^{2}}\frac{T^{n-1}_{o\_fin\ (iar,\theta+1,z)} - 2T^{n-1}_{o\_fin\ (iar,\theta,z)} + T^{n-1}_{o\_fin\ (iar,\theta-1,z)}}{\Delta\theta^{2}} + \ldots \\ & \frac{T^{n-1}_{o\_fin\ (iar,\theta,z+1)} - 2T^{n-1}_{o\_fin\ (iar,\theta,z)} + T^{n-1}_{o\_fin\ (iar,\theta,z-1)}}{\Delta z^{2}} - \frac{\dot{q}_{loss\_fin}}{k_{fin}}\end{aligned} \tag{3.29}$$

The convection heat transfer of collector fin surface to surrounding ($\dot{q}_{loss\_fin}$) can be calculated by Equation (3.30)

$$\dot{q}_{loss\_fin} = h_{i\_evac}(T^{n}_{o\_fin\ (iar,\theta,z)} - T^{n-1}_{air\_i\_evac}) \tag{3.30}$$

Where k_{fin} is thermal conductivity of collector fin (W/m-K), $T^{n-1}_{air\_i\_evac}$ is the air inside an evacuated tube at the previous time (K), h_{i_evac} is natural convection heat transfer

coefficient at the inner evacuated tube (W/m^2-K) (Cengel, 2004) that calculated from Equation (3.31)

$$Nu = h_{i\_evac}\frac{D_{o\_fin}}{k_{fin}} = \left\{0.60 + \frac{0.387Ra_D^{1/6}}{\left[1+\left(\frac{0.559}{Pr_{i\_evac}}\right)^{9/16}\right]^{8/27}}\right\}^2 \qquad Ra_D \le 10^{12} \tag{3.31}$$

The Rayleigh number (Ra_D) is given by

$$Ra_D = \frac{g\beta D_{o\_fin}^3\left(T_{o\_fin\ (iar,\theta,z)}^n - T_{am}^n\right)}{(\nu\alpha)_{air\_evac}} \tag{3.32}$$

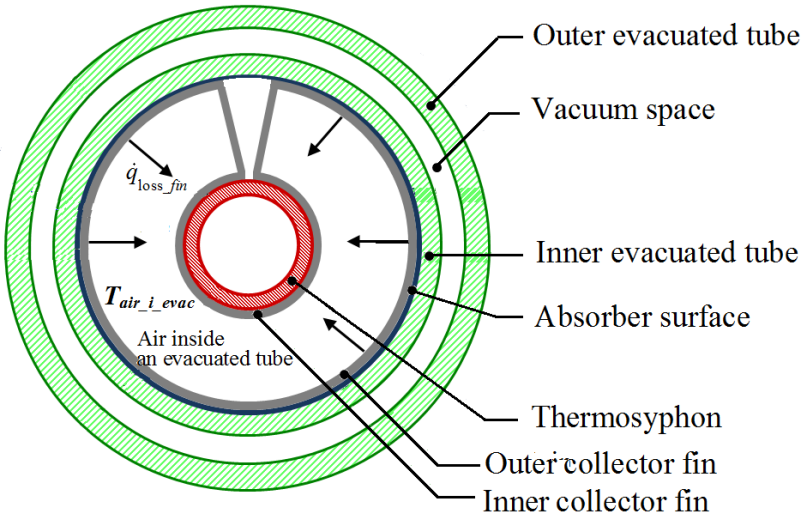

Figure 3.12 Cross-sectional views for describe the convection heat transfer of outer collector fin to the air inside an evacuated tube

From Figure 3.12 and the convection heat transfer in Equation (3.30) is used for calculating the air inside an evacuated at present time ($T_{air\_i\_evac}^n$) as

$$T_{air\_i\_evac}^n = \frac{\dot{q}_{loss\_fin}A_{o\_fin}(\Delta t)}{M_{air\_i\_evac}c_p} + T_{air\_i\_evac}^{n-1} \tag{3.33}$$

From Figure 3.5, the outer collector fin is connected by arm collector fin to inner collector fin. In this work, the arm collector fin is divided into five annual rings and 0.8 mm of radial step (Δr). Thus, the temperature of arm collector fin can be calculated by Equation (3.21).

For the inner collector fin, at the outside annual ring of inner collector fin has the heat convection from the outer collector fin by the air inside an evacuated tube. The temperature of outside annual rings of an inner collector fin at the present time can be calculated by:

$$\begin{aligned}\frac{T^{n}_{i\_fin\ (oar,\theta,z)} - T^{n-1}_{i\_fin\ (oar,\theta,z)}}{\alpha\Delta t} &= \frac{T^{n-1}_{i\_fin\ (oar+1,\theta,z)} - 2T^{n-1}_{i\_fin\ (oar,\theta,z)} + T^{n-1}_{i\_fin\ (oar-1,\theta,z)}}{\Delta r^{2}} + \ldots \\ &\frac{1}{\Delta r}\frac{T^{n-1}_{i\_fin\ (oar+1,\theta,z)} - T^{n-1}_{i\_fin\ (oar-1,\theta,z)}}{2\Delta r} + \ldots \\ &\frac{1}{(\Delta r)^{2}}\frac{T^{n-1}_{i\_fin\ (oar,\theta+1,z)} - 2T^{n-1}_{i\_fin\ (oar,\theta,z)} + T^{n-1}_{i\_fin\ (oar,\theta-1,z)}}{\Delta\theta^{2}} + \ldots \\ &\frac{T^{n-1}_{i\_fin\ (oar,\theta,z+1)} - 2T^{n-1}_{i\_fin\ (oar,\theta,z)} + T^{n-1}_{i\_fin\ (oar,\theta,z-1)}}{\Delta z^{2}} + \frac{\dot{q}_{loss\_fin}}{k_{fin}}\end{aligned} \tag{3.34}$$

While the temperature at the present time of another annual ring of inner collector fin is calculating by applied from Equation (3.21), it follows that:

$$\begin{aligned}\frac{T^{n}_{i\_fin\ (r,\theta,z)} - T^{n-1}_{i\_fin\ (r,\theta,z)}}{\alpha\Delta t} &= \frac{T^{n-1}_{i\_fin\ (r+1,\theta,z)} - 2T^{n-1}_{i\_fin\ (r,\theta,z)} + T^{n-1}_{i\_fin\ (r-1,\theta,z)}}{\Delta r^{2}} + \ldots \\ &\frac{1}{\Delta r}\frac{T^{n-1}_{i\_fin\ (r+1,\theta,z)} - T^{n-1}_{i\_fin\ (r-1,\theta,z)}}{2\Delta r} + \ldots \\ &\frac{1}{(\Delta r)^{2}}\frac{T^{n-1}_{i\_fin\ (r,\theta+1,z)} - 2T^{n-1}_{i\_fin\ (r,\theta,z)} + T^{n-1}_{i\_fin\ (r,\theta-1,z)}}{\Delta\theta^{2}} + \ldots \\ &\frac{T^{n-1}_{i\_fin\ (r,\theta,z+1)} - 2T^{n-1}_{i\_fin\ (r,\theta,z)} + T^{n-1}_{i\_fin\ (r,\theta,z-1)}}{\Delta z^{2}}\end{aligned} \tag{3.35}$$

From Equation (3.28) to Equation (3.35), the temperature of outer collector fin and inner collector fin at the present time are obtained. Moreover, temperature of an annual ring inside an inner collector fin ($T^{n}_{i\_fin\ (iar,\theta,z)}$) at the present

time is defined to be equal to the temperature of an annual ring outside an evaporator section ($T^{n}_{evap(oar,\theta,z)}$) for calculating the thermosyphon domain.

3.2.3.3 Thermosyphon domain

The evaporator section and the condenser section are divided into three annual rings. From the boundary condition, temperature of an annual ring outside the evaporator section ($T^{n}_{evap(oar,\theta,z)}$) is equal to temperature of an annual ring inside the inner collector fin ($T^{n}_{i\_fin\ (iar,\theta,z)}$). For another annual ring, temperature of the evaporator can be calculated at the present time ($T^{n}_{evap(r,\theta,z)}$) as follow:

$$\begin{aligned}\frac{T^{n}_{evap(r,\theta,z)}-T^{n-1}_{evap(r,\theta,z)}}{\alpha\Delta t} &= \frac{T^{n-1}_{evap(r+1,\theta,z)}-2T^{n-1}_{evap(r,\theta,z)}+T^{n-1}_{evap(r-1,\theta,z)}}{\Delta r^{2}} \\ &+\frac{1}{\Delta r}\frac{T^{n-1}_{evap(r+1,\theta,z)}-T^{n-1}_{evap(r-1,\theta,z)}}{2\Delta r} \\ &+\frac{1}{(\Delta r)^{2}}\frac{T^{n-1}_{evap(r,\theta+1,z)}-2T^{n-1}_{evap(r,\theta,z)}+T^{n-1}_{evap(r,\theta-1,z)}}{\Delta\theta^{2}} \\ &+\frac{T^{n-1}_{evap(r,\theta,z+1)}-2T^{n-1}_{evap(r,\theta,z)}+T^{n-1}_{evap(r,\theta,z-1)}}{\Delta z^{2}}\end{aligned} \tag{3.36}$$

Considering the condenser section in Figure 3.13, the working fluid in thermosyphon is evaporated and flow to the condenser section which flow is obstruct by the thermal resistance of film boiling and film condensation. Thus, the temperature of the evaporator at inside annual ring is obtained from Equation (3.36) and the temperature of an annual ring inside the condenser section ($T^{n}_{cond(iar,\theta,z)}$) can be calculated by Equation (3.37).

$$T^{n}_{cond(iar\theta,z)} = T^{n}_{evap(iar\theta,z)} - \left(Q_{syphon}\left(Z_3 + Z_7\right)\right) \tag{3.37}$$

Where Z_3 *and* Z_7 are the thermal resistance of film boiling and film condensation and $\dot{Q}_{syphon}$ is the remainder of thermal energy of thermosyphon at the evaporator section which can be considered by the energy balance in Figure 3.13(a) and calculated from Equation (3.38).

$$\dot{Q}_{syphon} = I_G A_{i\_evac}(\tau\alpha) - \dot{Q}_{loss\_evac} - \dot{Q}_{loss\_fin} \quad (3.38)$$

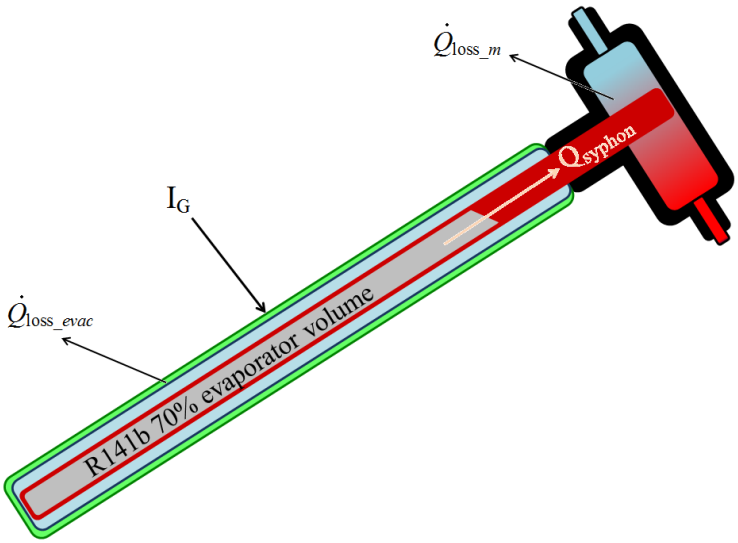

(a) energy balance of the evacuated tube collector

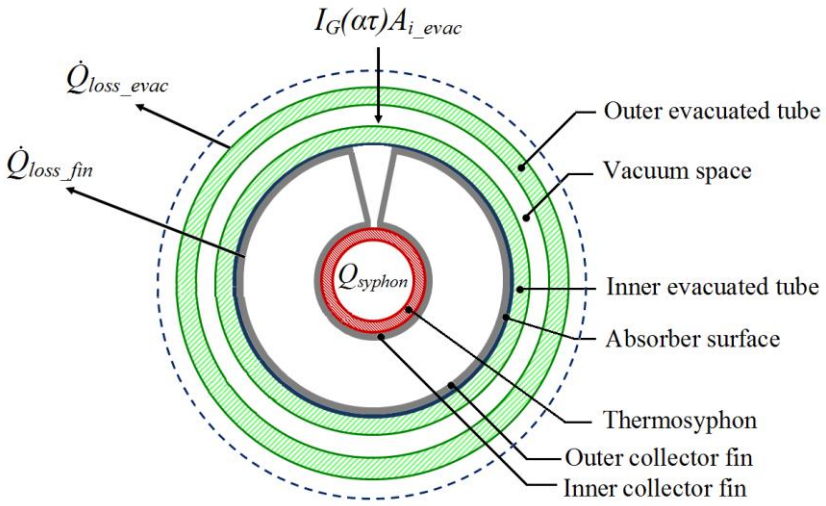

(b) cross-sectional views of the evacuated tube with thermosyphon

Figure 3.13 The energy balance and the cross-sectional views for the controlled surface of the evacuated tube at thermosyphon region

Equation (3.37) and Equation (3.38) obtained the temperature of an annual ring inside the condenser section ($T^{n}_{cond(iar,\theta,z)}$). Thus, temperature of another annual ring of condenser section can be expressed as

$$\frac{T^{n}_{cond(r,\theta,z)} - T^{n-1}_{cond(r,\theta,z)}}{\alpha\Delta t} = \frac{T^{n-1}_{cond(r+1,\theta,z)} - 2T^{n-1}_{cond(r,\theta,z)} + T^{n-1}_{cond(r-1,\theta,z)}}{\Delta r^{2}} + \frac{1}{\Delta r}\frac{T^{n-1}_{cond(r+1,\theta,z)} - T^{n-1}_{cond(r-1,\theta,z)}}{2\Delta r} + \frac{1}{(\Delta r)^{2}}\frac{T^{n-1}_{cond(r,\theta+1,z)} - 2T^{n-1}_{cond(r,\theta,z)} + T^{n-1}_{cond(r,\theta-1,z)}}{\Delta\theta^{2}} + \frac{T^{n-1}_{cond(r,\theta,z+1)} - 2T^{n-1}_{cond(r,\theta,z)} + T^{n-1}_{cond(r,\theta,z-1)}}{\Delta z^{2}} \quad (3.39)$$

From Equation (3.36) to Equation (3.39), evaporator ($T^{n}_{evap(r,\theta,z)}$) and condenser temperature ($T^{n}_{cond(r\theta,z)}$) at the present time are obtained.

3.2.3.4 Manifold domain

For the manifold and water storage tank, we are considered to be similar to the thermal resistance method. The heat accumulation in the condenser is transferred to water by the convective heat transfer as shown in Figure 3.7. The energy balance of the manifold as

$$\dot{Q}_{ST\_m} = \dot{Q}_{convect\_m} + \dot{Q}_{wi} - \dot{Q}_{wo} - \dot{Q}_{loss\_m} \quad (3.40)$$

Heat transfer rate of water ($\dot{Q}_{ST\_m}$) at the manifold can be calculated from

$$\dot{Q}_{ST\_m} = \frac{M_{w\_m}c_{p}(T^{n}_{w\_m} - T^{n-1}_{w\_m})}{\Delta t} \quad (3.41)$$

Substitution of Equation (3.41) by Equation (3.40), is obtain Equation (3.42)

$$\frac{M_{w\_m}c_{p}(T^{n}_{w\_m} - T^{n-1}_{w\_m})}{\Delta t} = \dot{Q}_{convect\_m} + \dot{Q}_{wi} - \dot{Q}_{wo} - \dot{Q}_{loss\_m} \quad (3.42)$$

Equation (3.42) is converted to calculate water temperature within the manifold at the present time ($T^{n}_{w\_m}$) as

$$T_{w\_m}^{n} = \frac{(\dot{Q}_{convect\_m} + \dot{Q}_{wi} - \dot{Q}_{wo} - \dot{Q}_{loss\_m})\Delta t}{M_{w\_m} c_p} + T_{w\_m}^{n-1} \tag{3.43}$$

The net heat rate of water at the manifold can be calculated by temperature difference of water inlet and outlet at the manifold multiplied by the water flow rate and by the specific heat of water, it follows that

$$\dot{Q}_{io\_m} = \dot{m}_w c_p (T_{wo\_m}^{n} - T_{wi\_m}^{n}) \tag{3.44}$$

The heat convection ($\dot{Q}_{convect\_m}$) of water can be calculated from the thermal energy of thermosyphon ($\dot{Q}_{syphon}$) which is transferred to water by the condenser section. This heat transfer of thermosyphon is obstructed by the thermal resistance between water and external surface of condenser section ($Z_{convect\_m}$) at the manifold, which can be expressed in Equation (3.45).

$$\dot{Q}_{convect\_m} = \dot{Q}_{syphon} Z_{convect\_m} \tag{3.45}$$

When $Z_{convect\_m}$ can be calculated from water flow rate by external flow cross cylinder.

Furthermore, heat loss of water within the manifold ($\dot{Q}_{loss\_m}$) to surrounding is calculated by natural convection heat transfer at the outer surface of the manifold cab be calculated by Equation (3.13).

3.2.3.5 Water storage tank

Heat is accumulated in water at the manifold and then flowed to the water storage tank. Applying energy balance on the controlled volume as shown in Figure 3.8, it follows that

$$\dot{Q}_{ST\_tank} = \dot{Q}_{wi\_tank} - \dot{Q}_{wo\_tank} - \dot{Q}_{loss\_tank} \tag{3.46}$$

The accumulated heat rate of water at storage tank ($\dot{Q}_{ST\_tank}$) can be calculated as follow

$$\dot{Q}_{ST\_tank} = \frac{M_{w\_tank} c_p (T_{w\_tank}^{n} - T_{w\_tank}^{n\text{-}1})}{\Delta t} \tag{3.47}$$

Substitution of Equation (3.47) by Equation (3.46), is obtain Equation (3.48)

$$\frac{M_{w\_tank} c_p (T^{n}_{w\_tank} - T^{n\text{-}1}_{w\_tank})}{\Delta t} = \dot{Q}_{wi\_tank} - \dot{Q}_{wo\_tank} - \dot{Q}_{loss\_tank} \quad (3.48)$$

Equation (3.48) is converted to calculate water temperature within the storage tank at the present time ($T^{n}_{w\_tank}$) as

$$T^{n}_{w\_tank} = \left(\frac{\left(\dot{Q}_{wi\_tank} - \dot{Q}_{wo\_tank} - \dot{Q}_{loss\_tank}\right)\Delta t}{M_{w\_tank} c_p} \right) + T^{n\text{-}1}_{w\_tank} \quad (3.49)$$

Where M_{w_tank} is water mass within the storage tank (kg), $T^{n}_{w\_tank}$ is temperature of water in the storage tank at the present time (^{o}C), $T^{n-1}_{w\_tank}$ is water temperature in the storage tank at the present time (^{o}C), and Δt is storage interval time (s).

For $\dot{Q}_{wi\_tank}$ and $\dot{Q}_{wo\_tank}$ are heat rate water inside and outside at the storage tank which is referred to the net heat rate of the storage tank ($\dot{Q}_{io\_tank}$) and it can be calculated from:

$$\dot{Q}_{io\_tank} = \dot{m}_w c_p (T^{n}_{wi\_tank} - T^{n}_{wo\_tank}) \quad (3.50)$$

Where $T^{n}_{wi\_tank}$ is the inlet water temperature at storage tank and $T^{n}_{wo\_tank}$ is the outlet water temperature at storage tank. In this work, the water temperature within storage tank ($T^{n}_{w\_tank}$) is assumed to be equal to the outlet water temperature of the storage tank at the same time as interval.

Heat loss of water storage tank to surrounding ($\dot{Q}_{loss\_tank}$) occurred from the temperature difference of water temperature in storage tank and ambient air temperature can be calculated by Equation (3.16). The resistance between inner surface of storage tank and ambient (K/W) which can be calculate as follow

$$Z_{tank} = \left(\frac{t_{tank}}{A_{tank} k_{tank}}\right) + \left(\frac{t_{ins}}{A_{ins} k_{ins}}\right) + \left(\frac{1}{h_{air} A_{ins}}\right) \quad (3.51)$$

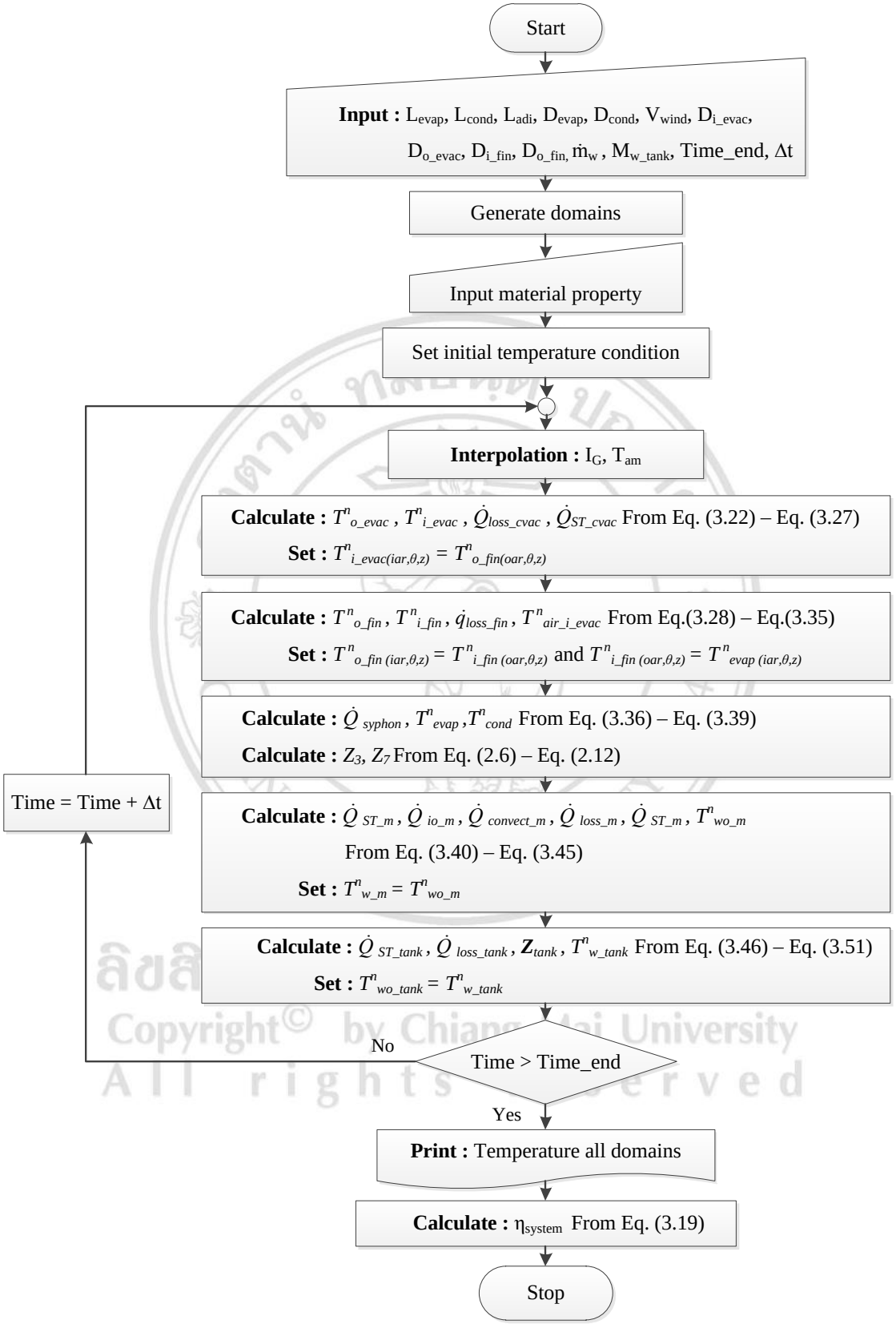

Figure 3.14 Flow chart of Explicit Finite Difference Method for the single evacuated tube solar water heater

Where t_{tank} is wall thickness of storage tank (m), t_{ins} is insulator thickness (m), A_{tank} and A_{ins} is area of the water storage tank or area of the insulated (m^2), k_{tank} and k_{ins} is the thermal conductivity of storage tank and insulated (W/m-K), respectively.

According to the mathematical model of evacuated tube solar water heater system, the domains are employed 60 s of time step (Δt), 15^o of circumferential step ($\Delta\theta$). The evacuated tube, the evaporator section, the adiabatic section, and collector fin are employed 100 mm of longitudinal step (Δz). Furthermore, the condenser section is employed 10 mm of longitudinal step. The flow chart of Explicit Finite Difference Method modeling of the single evacuated tube solar water heater with thermosyphon is described in Figure 3.14.

3.3 Results and Discussion

3.3.1 Experimental results

The single solar water heater in Figure 3.1 is tested based on the climate of Chiang Mai Province, Thailand on February 27, 2014. The solar intensity and ambient air temperature are also recorded on February 27, 2014 as shown in Figure 3.15. The experiment is carried out from 9:00 a.m. to 4:00 p.m.; solar intensity and air temperature influenced the system operation. The temperature of water is increased by adding solar intensity. It keeps increasing even though the solar intensity is decreased as shown in Figure 3.16.

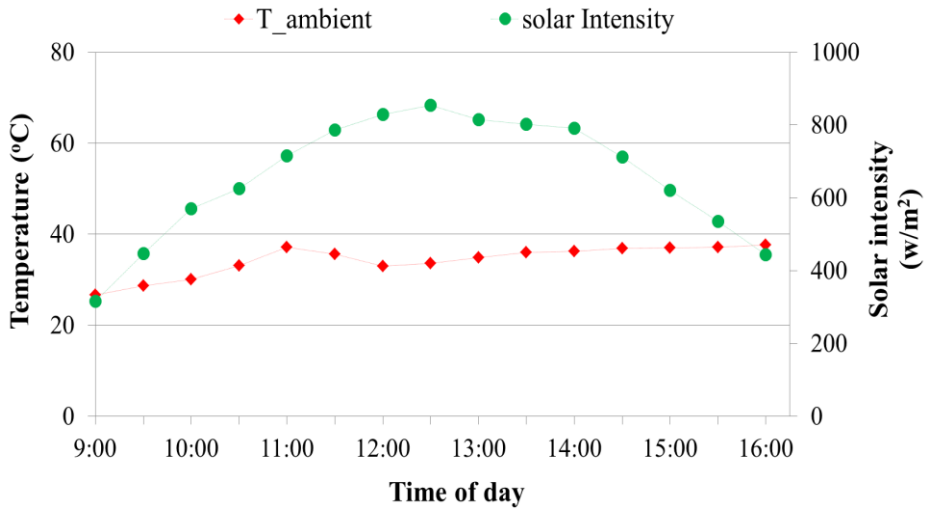

Figure 3.15 Variation of solar intensity and ambient temperature

The correlation between local time and temperature of hot water retrieved from industrial thermosyphon and R141b thermosyphon as shown in Figure 3.16. It can be concluded that hot water temperature of single evacuated tube of both industrial thermosyphon and R141b thermosyphon are obtained in a similar trend until local time reaches 4:00 p.m. Hot water's maximum temperature of the industrial thermosyphon and R141b thermosyphon is 58.23°C and 58.86°C at 4:00 p.m., respectively.

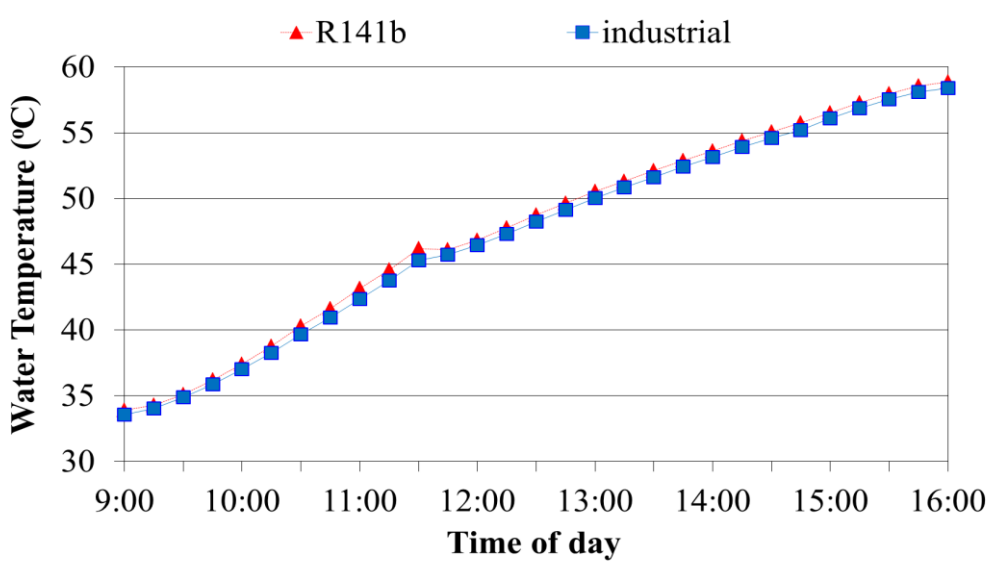

Figure 3.16 Variation of water temperature along with local time

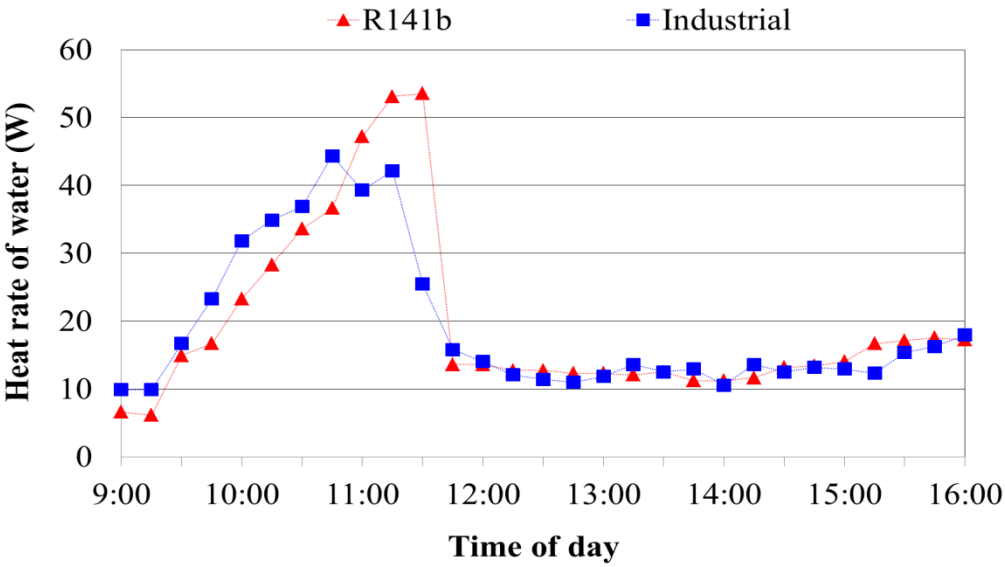

Figure 3.17 Variation of water heat rate along with local time

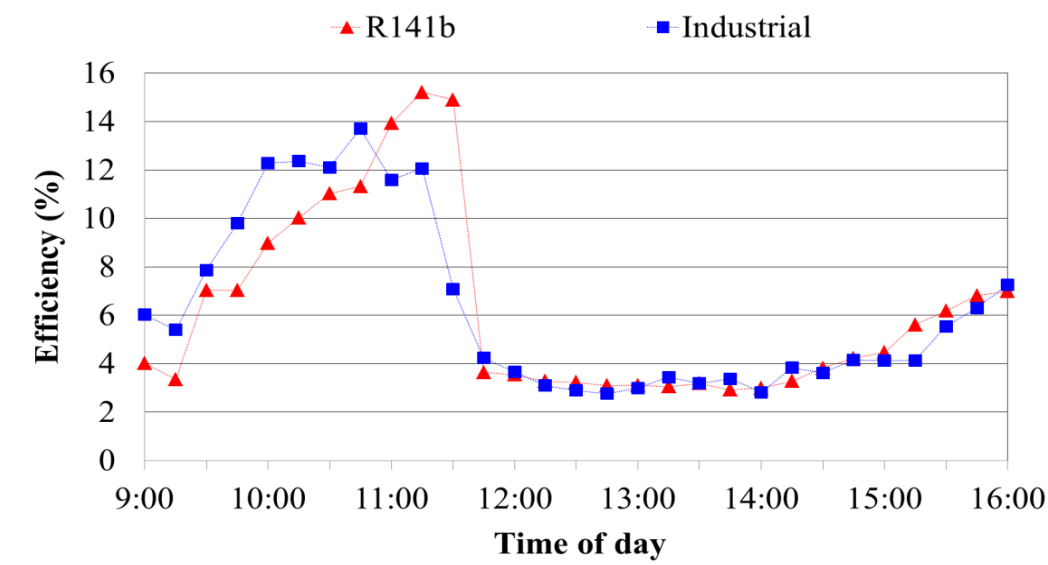

Figure 3.18 Variation of thermal efficiency along with local time

Heat transfer rate of single evacuated tube with industrial thermosyphon and R141b thermosyphon are shown in Figure 3.17. The results of both thermosyphons appear in a similar trend. It shows that water heat rate of the industrial thermosyphon gradually increases with its maximum value of 44.32 W at 10:30 a.m. while the R141b thermosyphon increases with its maximum value of 53.53 W at 11:30 a.m. After that, water heat rate of both thermosyphons are rapidly decreased until 12:30 p.m. because the different temperatures of hot water and limited ability in accumulating thermal energy of the water. Then, they are nearly constant to 3:00 p.m. after that are slightly increased to final time at 4:00 p.m.

The correlation between local time and thermal efficiency is shown in Figure 3.16. It is found that increased heat transfer rate of water will affect the thermal efficiency to be increased. Therefore, the maximum of thermal efficiency is 13.7% for the industrial thermosyphon at 10.45 a.m., whereas there is 15.2% for the R141b thermosyphon at 11.15 a.m. Thereafter, thermal efficiency of the system is rapidly decreased and becomes constant until the local time reaches 3:00 p.m. Finally, the thermal efficiency is then slightly increased. It can be noted that solar intensity influences thermal efficiency as higher solar intensity leads to lower thermal.

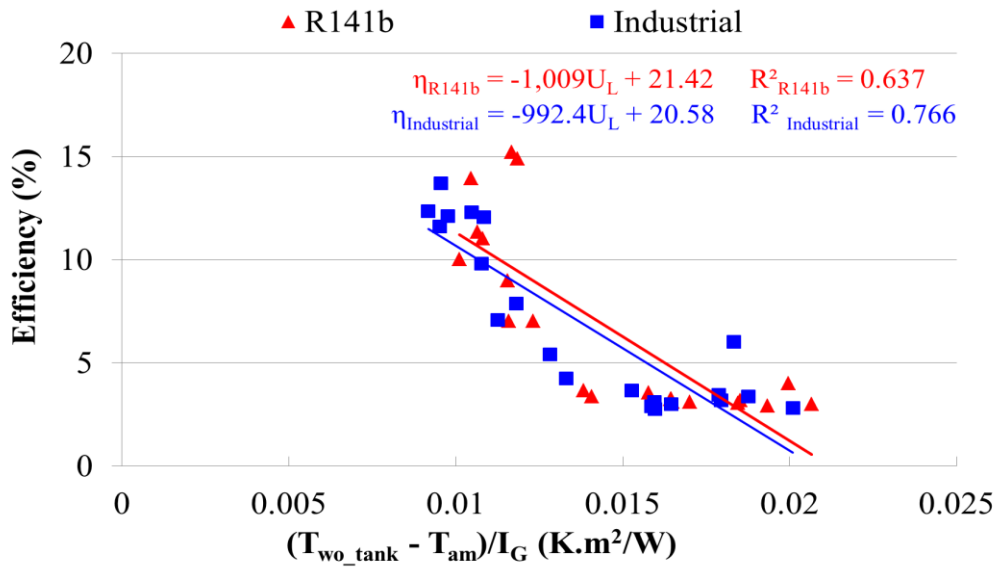

Figure 3.19 Correlation between $(T_{wo\_tank} - T_{am})/I_G$ and thermal efficiency

Therefore, the thermal efficiency as a condition of environmental is shown in Figure 3.19. It should be noted that environmental condition of $(T_{wo\_tank} - T_{am})/I_G$, where T_{wo_tank} is outlet water temperature of the storage tank and T_{am} is ambient temperature. In Figure 3.19, x-axis is $(T_{wo\_tank} - T_{am})/I_G$ while y-axis is the thermal efficiency. It is found that, the both thermosyphons result are in the same trend. For the industrial thermosyphon, the instantaneous maximum of thermal efficiency is 20.58% and overall heat transfer coefficient is 992.4 W/m^2-K. Furthermore, for the R141b thermosyphon, the instantaneous maximum of thermal efficiency and overall heat transfer coefficient is 21.42% and 1,009 W/m^2-K, respectively.

3.3.2 Validation of mathematical models

In order to develop the mathematical models for accurate prediction, solar intensity and ambient air temperature of the experiment are based on Chiang Mai province, Thailand on February 27, 2014 during 9:00 a.m. to 4:00 p.m. as shown in Figure 3.15. The models are used for simulating the operation of single evacuated tube solar water heater. Eventually, the results of mathematical models are presented in Figure 3.20 to Figure 3.25. Moreover, the accuracy of mathematical models can be proved validated by the experiment results.

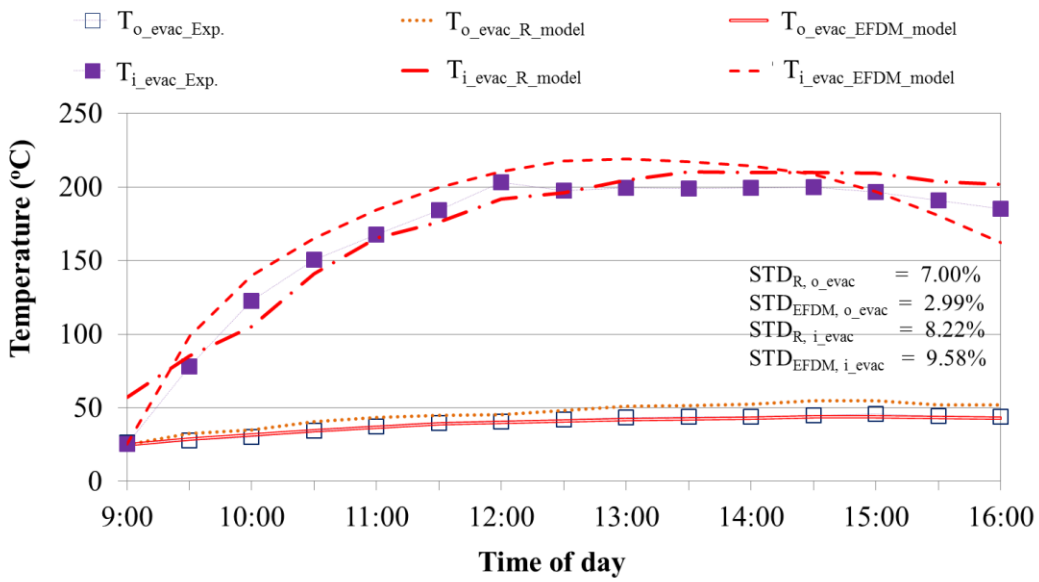

Figure 3.20 Temperature variation of evacuated tube along with local time

The correlation between local time and the evacuated tube temperatures is shown in Figure 3.20. Evacuated tube's outer temperature of the experiment, the thermal resistance method (R_model) and EFDM are slightly increased until 12:30 a.m. local time. After that, the temperatures are nearly constant along with local time. On the other hand, evacuated tube's inner temperature of the thermal resistance method, EFDM, and the experiment are gradually increased until 12:30 a.m. Thereafter, inner temperature of the thermal resistance method and the experiment is nearly constant at the final time when the inner temperature of EFDM is constant at 2:30 p.m. Then, it is slightly decreased because solar intensity is inputted in the EFDM during 2:30 p.m. to 4:00 p.m. The maximum inner temperature of evacuated tube of the thermal resistance method and EFDM are 210.32^{o}C at 1:30 p.m. and 218.97^{o}C at 12:30 a.m., respectively. Furthermore, maximum temperature of the experiment is 203.27^{o}C at 12:00 p.m. Therefore, evacuated tube's inner temperatures of these two models are similar in the experiment data.

The evaporator and condenser temperature of the experiment and mathematical models show in the same trend as displayed in Figure 3.21. It is found that, the evaporator temperature of the experiment and both mathematical models are rapidly increased until 1:00 p.m. and then the temperatures are nearly constant to the final time about 210.01^{o}C for the experiment, 218^{o}C for the thermal resistance method,

and 192.52°C for the EFDM. The maximum temperatures of evaporator are 209.28°C, 193.42°C, and 218.41°C for the experiment, thermal resistance method, and EFDM, respectively. The standard deviation (STD) compared to the experiment and mathematical models are 9.90% for the thermal resistance method and 5.62% for EFDM.

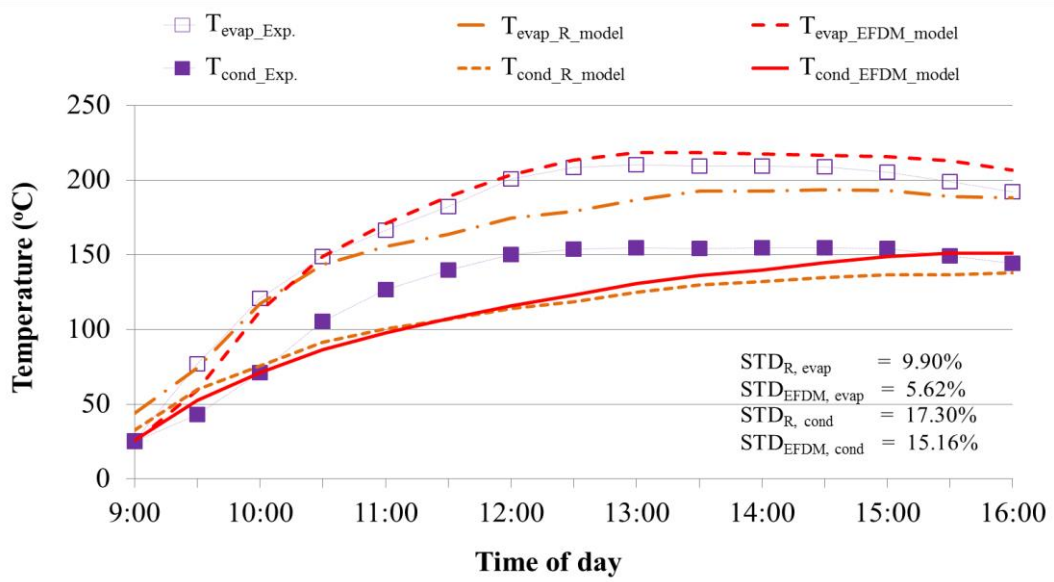

Figure 3.21 Variation of thermosyphon temperatures

According to the condenser temperature of the experiment, it is gradually increased until 12:00 p.m. local time, but becomes constant along with the standard local time of the day. The condenser temperatures of both mathematical models are gradually increased until 4:00 p.m. It can be seen that the experiment's temperature is higher than both models during 10:00 a.m. to 3:00 p.m. because the heat transferred in the experiment is less than in the models. This leads to heat stored in the condenser section. The condenser temperature is higher than in the models and it will affect the heat transfers in a small amount of water. Thus, the STD occurred at the condenser are 17.31% for the thermal resistance and 15.16% for EFDM.

The temperature of hot water in the experiment and mathematical models are presented in Figure 3.22. It can be noted that temperature of hot water in the experiment and in the models are likely to increase until the final time. Thus, the maximum

temperature of hot water occurred at the final time are 58.30°C for the experiment, 78.32°C for the thermal resistance method, and 68.51°C for EFDM.

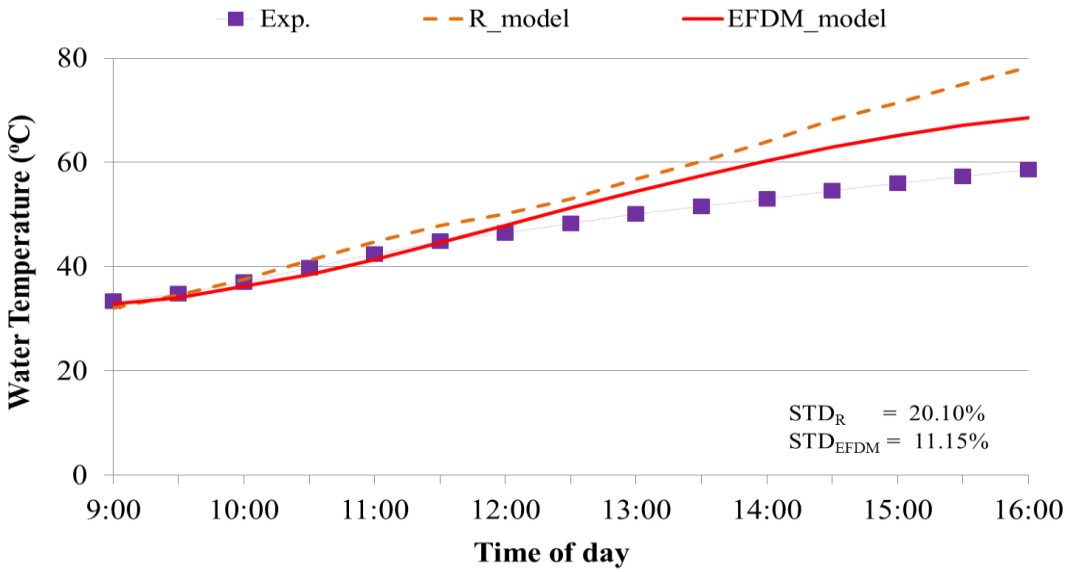

Figure 3.22 Temperature variation of hot water along the local time

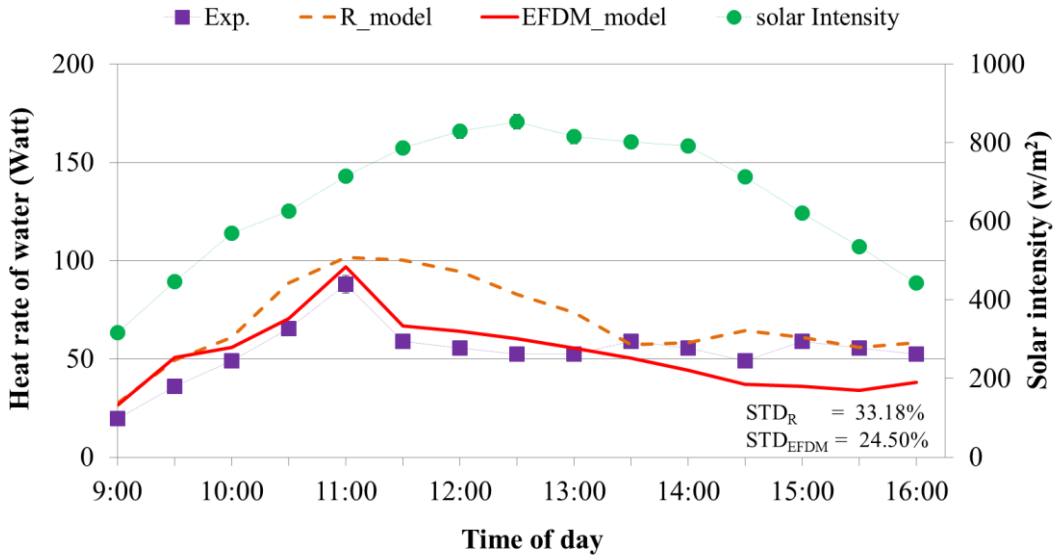

Figure 3.23 Heat rate of water along with local time

In Figure 3.22, hot water temperatures of the thermal resistance method and EFDM during 09:00 a.m. to 12:30 p.m. are close to the experimental result. Then, the hot water temperature of the experiment is lower than both models because heat

transferring ability at the condenser is less than the models while heat loss is higher than both models. For this reason, temperature of hot water in the experiment is lower. The results shown that, the STD of hot water temperature are 20.10% for thermal resistance method and 11.51% for EFDM.

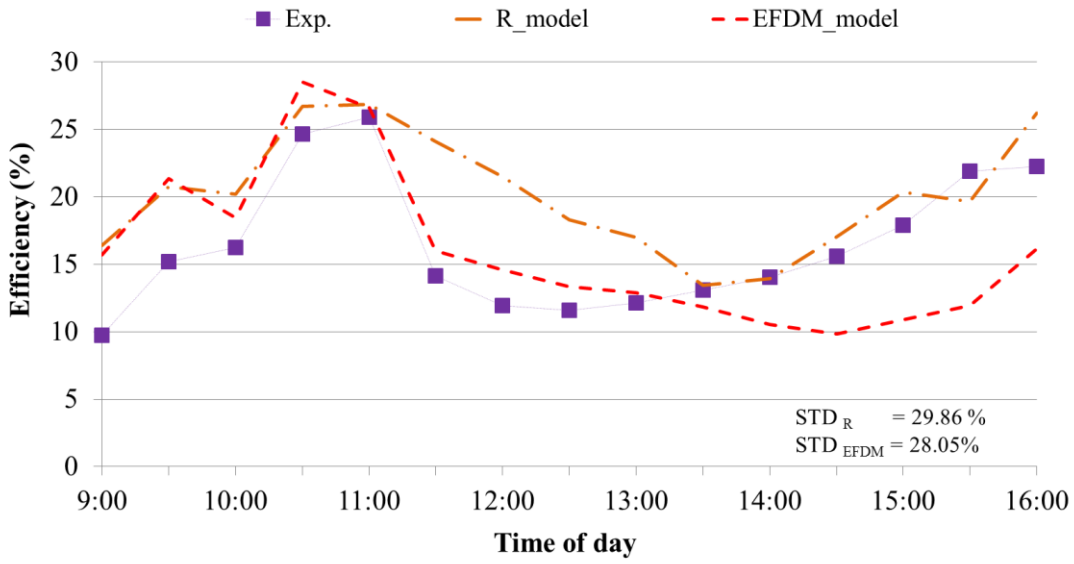

Figure 3.24 Variation of thermal efficiency along with local time

The variation of heat transfer rate of water is shown in following Figure 3.23. It can be concluded that heat transfer rate of water in the experiment and the two models tend to increase until 11:00 a.m. The maximum values are 88.01 W for the experiment, 101.37 W for thermal resistance method, and 97.04 W for EFDM. However, heat transfer rate of water is likely to decrease for the experiment while it is nearly constant for EFDM.

Thermal efficiency is illustrated in Figure 3.24. It can be noted that the solar intensity has influenced on the thermal efficiency of solar water heater. The increased solar intensity will affect the thermal efficiency and make it decreased. On the other hand, the lower solar intensity will affect the thermal efficiency and make it increased. The thermal efficiency in the experiment is from 11.70% to 23.22% in the morning and its highest value at 11:00 a.m. According to the results of the mathematical models, thermal efficiency of the models is increased from 15.70% to 25.61% for EFDM and

increased from16.42% to 26.85% for thermal resistance method. The STD of the thermal efficiency is 29.86% for thermal resistance method and 28.05% for EFDM.

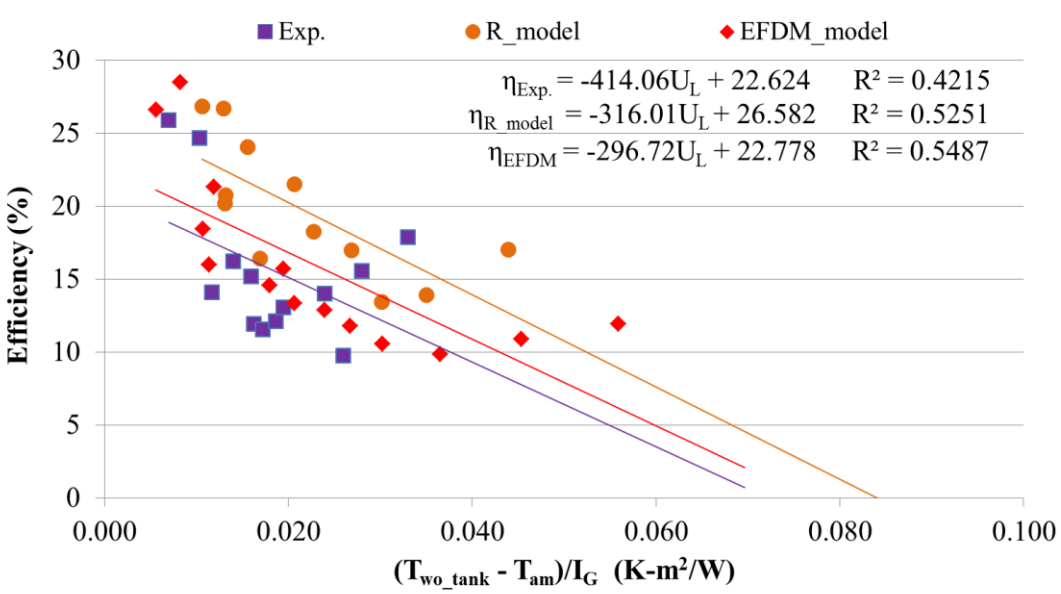

Figure 3.25 Relationship of $(T_{wo\_tank} - T_{am})/I_G$ and thermal efficiency

The correlation between $(T_{wo\_tank} - T_{am})/I_G$ and thermal efficiency are shown in Figure 3.25. It can be concluded that the thermal efficiency of single evacuated tube in the experiment, thermal resistance method, and EFDM are 22.62%, 26.58, and 22.77%, respectively. In addition, the overall heat transfer coefficient is 414.06 W/m^2-K for the experiment, 316.01 W/m^2-K for thermal resistance method, and 296.72 W/m^2-K for EFDM. Moreover, the coefficient of determination value is 0.42, 0.52 and 0.54 of the experimental result, the thermal resistance result, and EFDM result, respectively. Those coefficients of determination value are interpreted as the variable proportion of linear regression analysis in experimental that is explained by the model.

3.4 Conclusion

The mathematical models of single evacuated tube solar water heater with thermosyphon are established and validated accurate by the experiment results. The conclusions are as followings:

1) Thermal efficiency of the mathematical models is proved by the experimental result. It shows that the mathematical models are in good agreement with the experimental results. Moreover, the EFDM is shown accurate than the thermal resistance method about 16.73%.
2) The instantaneous thermal efficiency of single evacuated tube in the experiment, thermal resistance method, and EFDM are 22.47%, 29.39%, and 23.47%, respectively.
3) The maximum temperature of hot water in the experiment, thermal resistance method, and EFDM are 58.30^{o}C, 78.32^{o}C, and 68.51^{o}C, respectively. It should be noted that these temperatures occurred at the final time of the day.